Synthesis and luminescence properties of new nitridolithosilicate phosphor $La_4Ba_3Li_3Si_9N_{19}$: Pr^{3+} grown in Li flux

Rui-Xin Li,[a] Xiao-Ming Wang, *[a] Shi-Rui Zhang,[a] Xue Gu,[a] Zu-Pei Yang,[b] and Huan Jiao *[a]

Electronic Supplementary Information (ESI):

Materials and synthesis.

Based on the sensitivity of the starting materials to oxygen and moisture, all experimental operations were performed under a glovebox filled with argon conditions (Beijing Mikrouna, O_2 < 1 ppm, H_2O < 1 ppm). The single crystals of $La_4Ba_3Li_3Si_9N_{19}$ were synthesized from Li_3N (0.48 mmol, Hebei LiFu, 99.9%), LaN (1.50 mmol, Yantai Xierde, 99%), Ba_3N_2 (0.50 mmol), α-Si_3N_4 (1.65 mmol, Alfa Aesar, 99.9%)，15mmol Li was added as flux. The powder reactants were ground for 30 minutes and placed in a tantalum ampule (wall thickness 0.5 mm, internal diameter 10 mm, length 150 mm), which was arc-welded under a pressure of 1 bar purified argon. The reaction mixture then heated to 1400℃ within 2h, maintained for 20h, finally cooled down to 1000℃ and quenched to room temperature. Powder samples of $La_4Ba_3Li_3Si_9N_{19}$ were synthesized from Li (12 mmol), Li_3N (0.40 mmol, Hebei LiFu, 99.9%), LaN (1.50 mmol, Yantai Xierde, 99%), Ba_3N_2 (0.38 mmol, Yantai Xierde, 99%), α-Si_3N_4 (1.08 mmol, Alfa Aesar, 99.9%) and PrN (Alfa Aesar, 99.9%) was added as an activator. Raw materials were mixed in an agate mortar and then filled into tungsten crucibles, then the crucibles were positioned in the middle of a tube furnace under a reductive atmosphere of 6:94 (volume) H_2/N_2 and heated to 1550℃ within 2 h. After being maintained at 1550℃ for 6h, the furnace was cooled down to 1000℃ for 3h and finally cooled to room temperature by switching off the furnace. The body colors of the host sample and Pr^{3+} doped samples are both light yellow.

Characterization

Single-Crystal X-ray Diffraction. The single crystals of $La_4Ba_3Li_3Si_9N_{19}$ were isolated from the powder samples and mounted on a 50 μm CryoLoop (Hampton). Single-Crystal X-ray diffraction data were collected on Rigaku diffraction (XtaLAB Synergy-R) with a rotating anode X-ray source (Cu Kα radiation). The crystal structure of $La_4Ba_3Li_3Si_9N_{19}$ was solved by direct methods (SHELXT)[1] and refined by full-matrix least-squares methods (SHELXL)[2]. All the atom sites were refined with anisotropic displacement parameters. Further details of $La_4Ba_3Li_3Si_9N_{19}$ crystal structure investigation can be available from the Cambridge Crystallographic Data Centre (CCDC) on quoting the depository number CCDC code 2119741.

Powder X-ray Diffraction (PXRD). PXRD data were collected using a Cu source from a Rigaku

MiniFlex600 diffractometer (Japan). The data were recorded over a 2θ range from 5° to 120° at intervals of 0.01° and a total data collection time of 2 h. Rietveld refinements on PXRD data were carried out by Topas 5.0 software[3, 4].

Scanning Electron Microscopy (SEM). To determine the morphology and chemical analysis of the compound, SEM (Philips-FEI Quanta 25) and an attached energy dispersive X-ray spectrometer (EDAX, Element System) were used with TEAM software. The product particle was marginally placed on an adhesive conductive carbon pad.

Transmission Electron Microscopy (TEM). TEM was used to examine fine details of the samples' morphology utilizing a Thermo Fisher Scientific Talos F200i field emission TEM. The sample was prepared by evaporation in the air of a droplet of the powders dispersed in absolute alcohol onto ultra-thin carbon films supported on copper TEM grids.

UV/vis Spectroscopy. The ultraviolet–visible (UV–vis) diffuse reflectance (DR) spectra were measured on a Lambd 1050 UV-vis-NIR spectrophotometer (Perkin-Elmer), while the white powder $BaSO_4$ was used as a standard material. Converting the measured reflectance spectrum to a pseudo-absorption spectrum was achieved by using the Kubelka–Munk function[5]:

$$\left[F(R_\infty)\right] = \frac{(1-R)^2}{2R}$$

(with R being the reflectance). The values of $[F(R_\infty h\nu)]^n$ with n = 1/2 for an indirect allowed transition are plotted as a function of the incident photon energy (hν).

Density Functional Theory. All calculations were performed with the Cambridge Serial Total Energy Package (CASTEP) code, in which the plane-wave basis set was chosen for the expansion of valance–electron wave functions at the local density approximation (LDA) level. The crystal structure was optimized by using the Broyden-Fletcher-Goldfarb-Shannon (BFGS) method. Structural relaxations of the unit cells of $La_4Ba_3Li_3Si_9N_{19}$ were done with a convergence criteria of 1.0×10^{-7} eV/atom for total energies. The energy cutoff of plane wave basis was set to 340 eV and Γ-centered *k*-meshes (4 × 4 × 2) produced from the method of Monkhorst-Pack grid (separation ~0.04 $Å^{-1}$) were used for sampling the Brillouin zone. Band structure calculations were performed on the basis of the primitive cell. Furthermore, the co-occupied (La2, La3) and half occupied (Si1, Li1, N10) were separated by reducing the space group symmetry to *P*1 (No.1) for avoiding calculation error.

Luminescence. The photoluminescence (PL) and photoluminescence excitation (PLE) spectra were measured at room temperature using a Hitachi F-7000 fluorescent spectrophotometer (Japan) with a 150 W Xe lamp as the excitation source. The spectrum correction was applied and color

coordinates were calculated by using the spectra data. High temperature-dependent PL spectra of $La_{3.99}Ba_3Li_3Si_9N_{19}$: $0.01Pr^{3+}$ were investigated between 300K and 500K using a TAP-02 high-temperature fluorescence attachment. In order to evaluate the thermal stability of the material more intuitively through the data, the Arrhenius equation can be used[6]:

$$\frac{I_T}{I_0} = [1 + Dexp(\frac{-E_a}{KT})]^{-1}$$

where $I_{(0,\ T)}$ stands for the emission intensity at initial temperature and the temperature monitoring, D means a constant and K = 8.617×10-5 eV K^{-1} (Boltzmann constant), E_a is the activation energy. The decay curves were analyzed by fluorescence spectrophotometer with a 150 W microsecond pulsed lamp as the excitation source on the Edinburgh FLS1000 fluorescence spectrophotometer. The curve of the Pr^{3+} activated phosphor can be well fitted by a second-order exponential function[7, 8]:

$$I(t) = I_0 + A_1\exp\left(-\frac{t}{\tau_1}\right) + A_2\exp\left(-\frac{t}{\tau_2}\right) \quad (1)$$

$$\tau_{ave} = (A_1\tau_1^2 + A_2\tau_2^2)/(A_1\tau_1 + A_2\tau_2) \quad (2)$$

where $I(t)$ stands for the emission intensity at the temperature monitoring, I_0 means the background intensity, A_1 and A_2 are the fitting constants, τ_1, τ_2 and τ_{ave} refers to the short, long and average lifetime respectively.

Table of Contents

Table S1. Atomic coordinates, Wyckoff positions, equivalent displacement parameters, and site occupancies of $La_4Ba_3Li_3Si_9N_{19}$.

Atom	*Wyck.*	x	y	z	*S.o.f.*	U_{eq}/ Å^2
Ba1	4*c*	1	0.6011(4)	0.75	1.0	0.0051(1)
Ba2	8*f*	1	0.1733(3)	0.5220(6)	1.0	0.0180(1)
La1	8*e*	0.7267(6)	0.50	0.50	1.0	0.0245(1)
La2	8*g*	0.7068(5)	0.3080(3)	0.75	0.2	0.0196(1)
La3	8*g*	0.7265(1)	0.2791(1)	0.75	0.8	0.0123(3)
Li1	8*f*	0.50	0.6007(1)	0.1230(3)	0.5	0.0102(1)
Li2	8*g*	0.2024(1)	0.5650(9)	0.25	1.0	0.0140(3)
Si1	8*f*	0.50	0.5462(2)	0.2231(3)	0.5	0.0063(4)
Si2	8*g*	0.3418(2)	0.4050(1)	0.25	1.0	0.0063(4)
Si3	16*h*	0.1610(1)	0.3293(8)	0.0255(1)	1.0	0.0056(3)
Si4	8*f*	0	0.4322(1)	-0.1105(2)	1.0	0.0056(4)
N1	8*f*	0	0.3057(4)	0.0817(7)	1.0	0.0076(1)
N2	8*d*	0.25	0.25	0	1.0	0.0102(1)
N3	4*c*	0.50	0.3609(6)	0.25	1.0	0.0080(9)
N4	16*h*	0.2483(5)	0.3801(3)	0.1272(4)	1.0	0.0080(9)
N5	8*g*	0.3554(8)	0.4986(4)	0.25	1.0	0.0160(1)
N6	16*h*	0.1494(5)	0.3822(3)	-0.0996(5)	1.0	0.0083(1)
N7	4*b*	0	0.50	0	1.0	0.0110(2)
N8	4*c*	0	0.4729(5)	-0.25	1.0	0.0051(1)
N9	4*c*	0.50	0.6322(7)	0.25	1.0	0.0290(3)
N10	8*f*	0.50	0.5469(1)	0.0621(1)	0.5	0.0196(1)

Table S2. Anisotropic displacement parameters (U_{iy} in Å^2) of $La_4Ba_3Li_3Si_9N_{19}$ with standard deviations in parentheses.

Atom	U^{11}	U^{22}	U^{33}	U^{12}	U^{13}	U^{23}
Ba1	0.004(1)	0.004(3)	0.006(1)	0.000(3)	0.000(7)	0.000(6)
Ba2	0.004(1)	0.016(3)	0.032(4)	0.000(5)	0.000(1)	0.016(2)
La1	0.008(3)	0.014(2)	0.050(4)	0.000	0.000(5)	-0.016(3)
La2	0.008(1)	0.044(3)	0.006(2)	0.006(2)	0.000(1)	0.000(1)
La3	0.014(1)	0.017(5)	0.005(2)	-0.005(1)	0.000(1)	0.000(1)
Li1	0.008(3)	0.011(3)	0.012(3)	0.003(3)	0.004(3)	0.005(3)
Li2	0.023(9)	0.012(7)	0.006(7)	0.002(7)	0.000(1)	0.000(1)
Si1	0.005(1)	0.007(2)	0.006(2)	-0.001(3)	0.000(5)	0.000(3)
Si2	0.005(1)	0.007(1)	0.006(2)	-0.001(3)	0.000(1)	0.000(6)
Si3	0.004(1)	0.005(1)	0.006(3)	0.001(5)	-0.001(4)	0.001(2)
Si4	0.005(1)	0.006(2)	0.004(3)	0.000(6)	0.000(1)	0.001(8)
N1	0.006(2)	0.008(3)	0.009(3)	0.000(1)	0.000(6)	0.003(3)
N2	0.008(1)	0.011(3)	0.012(3)	0.003(3)	0.004(3)	0.005(3)
N3	0.005(2)	0.010(2)	0.009(2)	0.000(5)	0.000(5)	0.000(1)
N4	0.005(2)	0.010(2)	0.009(2)	0.000(7)	0.000(1)	0.000(5)
N5	0.007(4)	0.008(3)	0.033(5)	0.001(3)	0.000(6)	0.000(1)
N6	0.007(2)	0.007(2)	0.011(2)	0.001(6)	0.001(2)	0.001(8)
N7	0.011(5)	0.009(5)	0.013(5)	0.000(6)	0.000(1)	-0.002(4)
N8	0.004(4)	0.004(4)	0.008(5)	0.000(3)	0.000(3)	0.000(3)
N9	0.017(6)	0.011(6)	0.059(8)	0.000(5)	0.000(7)	0.000(5)
N10	0.008(2)	0.044(3)	0.006(3)	0.006(2)	0.000(6)	0.000(3)

Table S3. Selected bond lengths and angles of $La_4Ba_3Li_3Si_9N_{19}$.

Bond	length(Å)	Bond	length(Å)
Si4—N8	1.742 (5)	N5—Li2	1.920 (6)
Si4—N6	1.722 (5)	N5—Si1	1.681 (8)
Si4—N7	1.758 (2)	N9—Si1	1.602 (6)
Si2—N3	1.737 (5)	N9—Li1	1.540 (3)
Si2—N4	1.719 (5)	Si1—N10	1.818 (4)
Si2—N5	1.716 (8)	N6—Li2	2.021 (7)
Si3—N6	1.715 (5)	N10—Li1	1.200 (4)
Si3—N2	1.712 (6)	Si3—N1	1.744 (4)
Si3—N4	1.703 (5)	N8—Li2	2.087 (3)
Bond	**Angle(deg)**	**Bond**	**Angle(deg)**
N8—Si4—N7	109.9 (3)	Li1—N9—Si1	57.2 (2)
N6—Si4—N8	106.9 (2)	N9—Si1—N5	118.2 (3)
N6—Si4—N7	108.8 (5)	N9—Si1—N10	100.5 (7)
N4—Si2—N3	110.2 (2)	Li1—N10—Si1	55.4 (3)
N5—Si2—N3	113.2 (4)	N5—Si1—N10	100.6 (4)
N5—Si2—N4	107.7 (2)	Si3—N4—Si2	162.0 (3)
N6—Si3—N1	112.3 (3)	Si1—N5—Si2	125.5 (5)
N2—Si3—N6	111.7 (5)	Si1—N5—Li2	108.8 (6)
N2—Si3—N1	107.8 (2)	N10—Li1—N9	147.0 (3)
N4—Si3—N6	106.3 (3)	N4—Si3—N2	108.8 (4)

Table S4. The Rietveld refinement of $La_4Ba_3Li_3Si_9N_{19}$ powder XRD data.

Chemical formula	$La_4Ba_3Li_3Si_9N_{19}$
Crystal system	Orthorhombic
Space group	*Cmcm* (No.63)
a (Å)	9.73642 (19)
b (Å)	18.2991 (4)
c (Å)	11.3100 (2)
Cell volume ($Å^3$)	2015.08 (2)
Z	4
Radiation	Cu Kα
Diffractometer	Rigaku MiniFlex 600
Structure refinement	Topas 5
Temperature (K)	297
2ϑ range (°)	5 - 120
Step size (°)	0.01
Profile function	PVⅡ
R_p	5.70
R_{wp}	7.49
R_{exp}	4.08
GOF	1.84

Table S5. Results in atom% from 10 EDX point-measurements of $La_4Ba_3Li_3Si_9N_{19}$.

Measurement	La	Ba	Si	N
1	10.10	7.89	21.85	60.16
2	8.51	6.60	19.73	65.17
3	9.85	7.84	21.99	60.32
4	8.76	6.90	20.28	64.06
5	8.17	6.12	19.46	66.25
6	8.49	6.98	19.84	64.69
7	9.81	7.43	21.58	61.18
8	9.82	7.60	22.38	60.20
9	8.06	6.20	19.26	66.48
10	8.90	7.03	20.47	63.60
Average	9.04	7.06	20.68	63.21

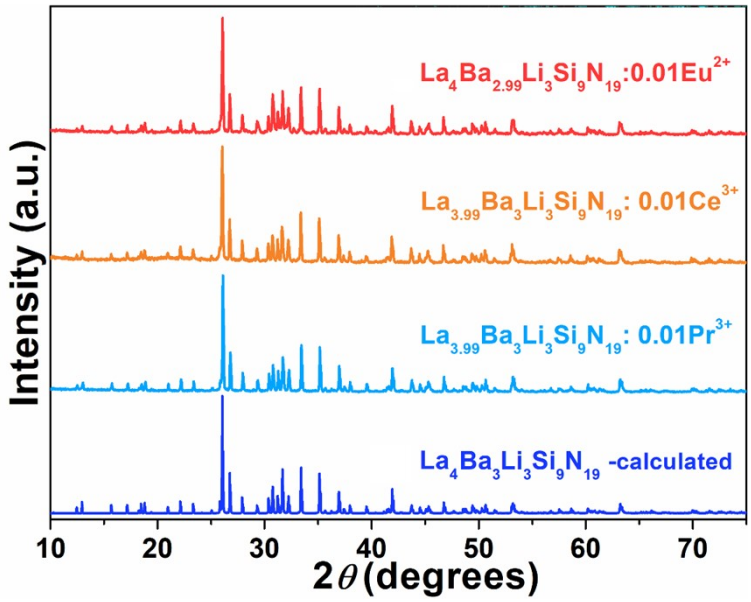

Fig. S1 The XRD patterns of Eu^{2+}, $Ce^{3+}$and Pr^{3+} doped $La_4Ba_3Li_3Si_9N_{19}$.

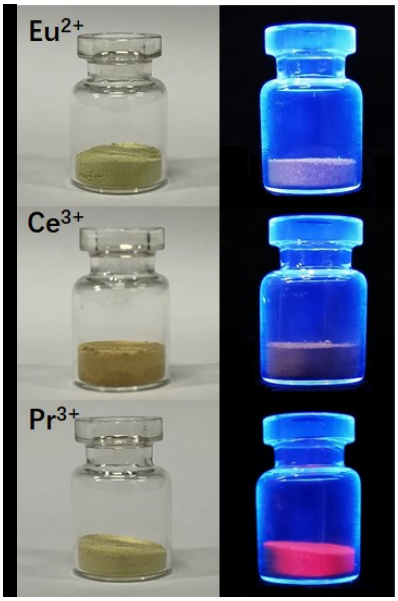

Fig. S2 The pictures of Eu^{2+}, Ce^{3+} and Pr^{3+} doped $La_4Ba_3Li_3Si_9N_{19}$ powder samples under daylight (a) and 365 nm UV excitation (b).

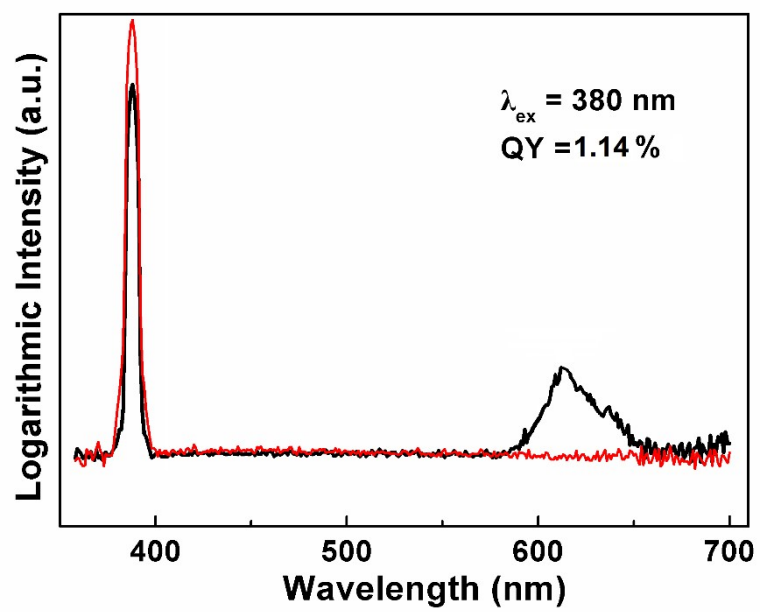

Fig. S3 The quantum efficiency (QE) of $La_{3.99}Ba_3Li_3Si_9N_{19}$: $0.01Pr^{3+}$ phosphor.

Reference

1. G. M. Sheldrick, *Acta Cryst.*, 2015, **A71**, 3-8.
2. G. M. Sheldrick, *Acta Cryst.*, 2008, **A64**, 112-122.
3. R. W. Cheary, A. A. Coelho, J. P. Cline, Res. Natl. Inst. Stand. Technol, 2004, 109, 1-25.
4. B. H. M. RIETVELD, *J. Appl. Cryst.* , 1969, **2**, 65-71.
5. R. López and R. Gómez, *J Sol-Gel Sci Technol, 2012*, **61**, 1-7.
6. Y. Li, Q. Wu, X. Wang, J. Ding, Q. Long and Y. Wang, *RSC Adv.*, 2014, **4**, 63569-63575.
7. C. Ji, T.-H. Huang, Z. Huang, J. Wen, W. Xie, X. Tian, T. Wu, H. He and Y. Peng, *J. Lumin.*, 2019, **216**.
8. C. Ji, Z. Huang, J. Wen, J. Zhang, X. Tian, H. He, L. Zhang, T.-H. Huang, W. Xie and Y. Peng, *J. Alloy. Compd.*, 2019, **788**, 1127-1136.